Sustainable Cities and Society 137 (2026) 107107

Contents lists available at ScienceDirect

Sustainable Cities and Society

journal homepage: www.elsevier.com/locate/scs

Unsupervised clustering approach to residential typo-morphologies across multiple cities for urban heat vulnerability assessment

Maha Habib [a,*], Doruntina Zendeli [b], Marjolein van Esch [a], Wim J. Timmermans [c], Maarten van Ham [a]

[a] Department of Urbanism, Faculty of Architecture and the Built Environment, Delft University of Technology, Julianalaan 134, 2628 BL, Delft, The Netherlands
[b] Department of Architecture and Urban Studies, Politecnico di Milano, Via Bonardi 3, 20133 Milan, Italy
[c] Department of Water Resources, Faculty of Geo-Information Science and Earth Observation, University of Twente, Hallenweg 8, 7522 NH, Enschede, The Netherlands

ARTICLE INFO

Dataset link: Clustering Approach to Residential Typo-morphologies Across Multiple Dutch Cities for Urban Heat Vulnerability Assessment (Original data)

Keywords:
Data-driven
Urban morphology
Local climate zone
Urban heat island
Climate adaptation

ABSTRACT

Residential environments are central to addressing urban heat stress for vulnerable populations and are prime target areas for implementing climate adaptation strategies. The reliance on urban heat island (UHI) intensity mapping alone has been argued to provide limited guidance for adaptation efforts, whereas linking heat patterns to the built environment characteristics through frameworks such as Local Climate Zones (LCZ) provides actionable insights for developing neighborhood cooling strategies. However, the widely used LCZ maps have a few limitations, such as misrepresenting variation within types because they cannot account for sub-classes beyond the standardized framework. This paper presents an unsupervised clustering approach to identify residential typo-morphologies across 99 Dutch cities, enhancing their relevance for urban heat vulnerability assessments. The analysis reveals that five morphological and canopy parameters (FSI, GSI, OSR, H_{avg}, and FVC) selected from 17 parameters are sufficient to identify nine distinct residential typo-morphologies relatable to LCZs within 100 m × 100 m grid cells. The evaluations demonstrate that our approach detects underrepresented LCZ types and reveals new sub-classes absent from standard LCZ classifications. Key findings include detection of high-density areas (LCZ 4_2) reflecting recent urban densification with one of the highest UHI_{max} next to LCZ 2 (4.2–4.9 K), and vegetation-differentiated variants within sparse and low-rise categories LCZ 9_D and LCZ 6_D, distinguished by distinctive UHI_{max} (0.5–0.7 K) higher compared to their reference base types. Notably, tree coverage remains low across low-rise and compact typo-morphologies, revealing substantial opportunities for greening interventions. This data-driven refinement preserves LCZ's global comparability while considering local specificity, providing improved frameworks to inform targeted climate adaptation strategies in residential environments.

1. Introduction

The past decade has been the warmest on record, with global temperatures rising by 1.54 (±0.13) °C above pre-industrial levels (Kennedy et al., 2024). At the same time, climate change is increasing the frequency and intensity of extreme heat events, leading to serious health risks globally. European cities face heightened vulnerability due to aging populationsand a lack of acclimatization to high temperatures, with heat-related mortality projected to rise significantly as heatwaves become more frequent (IPCC 2023; García-León et al., 2024). Moreover, the impacts of heat exposure are more pronounced in cities because of the urban heat island (UHI) effect, where urban areas are warmer than their surrounding rural counterparts (Oke, 1978).

The UHI effect intensifies heat exposure and risk, particularly for vulnerable populations, such as the elderly, chronically ill, and those with limited mobility, who are often bound to their place of residence (Kenny et al., 2024; Palme & Salvati, 2021). Understanding UHI variation across residential neighborhoods is therefore critical for targeting heat adaptation efforts, especially for those at risk. Morphological parameters, such as building height, density, and canyon orientation play a key role in modulating temperature through shading, heat storage, and the trapping of infrared radiation (Masson et al., 2020; Oke, 1978; Souch and Grimmond, 2006). At night, dense urban areas retain more heat and restrict airflow within street canyons, limiting cooling (Li et al., 2020;

* Corresponding author.
E-mail address: mmoustafahabib@tudelft.nl (M. Habib).

https://doi.org/10.1016/j.scs.2025.107107
Received 3 June 2025; Received in revised form 13 October 2025; Accepted 29 December 2025
Available online 1 January 2026

Thravalou et al., 2021). The effectiveness of heat mitigation and adaptation measures depends on how urban form influences heat retention and whether sufficient space is available to implement interventions (Bassolino et al., 2021; Rahmani and Sharifi, 2025; Villaverde et al., 2024).

To support targeted interventions, researchers, urban planners and practitioners can benefit from standardized frameworks for classifying residential typo-morphologies, which refers to the combinations of building density, configuration, and land cover characteristics that shape local heat vulnerability within cities. It has been argued that relying on UHI intensity maps alone offers limited guidance for heat adaptation, whereas linking heat patterns to the built environment offers stakeholders insights for designing neighborhood cooling strategies (Alexander and Mills, 2014; Martilli et al., 2020). One widely established effort to do so is by leveraging the Local Climate Zones (LCZ) classification developed by Stewart and Oke (2012), which provides a standardized framework that categorizes neighborhoods into 10 built and 7 natural types based on surface roughness, land cover, and geometry, all of which shape their thermal behavior. These categories were developed to enhance comparability of intra-urban UHI assessments beyond traditional urban–rural contrast.

Although LCZ mapping is a standard tool in urban climate studies (Bechtel and Daneke, 2012; Ching et al., 2018), it faces three key limitations for residential heat vulnerability assessment. First, the LCZ maps does not explicitly encode land use or function, limiting their ability to distinguish residential areas from commercial areas. Second, accuracy challenges arise from supervised classification relying on crowdsourced and satellite data, which vary in quality and contributor expertise (Bechtel et al., 2019), leading to inconsistencies in LCZ mapping efforts (Eldesoky et al., 2019; Geletič and Lehnert, 2016; Hidalgo et al., 2019; Rodler and Leduc, 2019; Verdonck et al., 2017). In the Netherlands, for example, certain built LCZ types (e.g., LCZ 2 and LCZ 4, which largely consist of historical and post-war buildings) are severely underrepresented or nearly absent (see Table A.1). Third, the framework's predefined categories limits the possibility of identifying residential sub-classes that reflect local or regional variations in urban form, a limitation acknowledged by Stewart and Oke (2012). In response, researchers have manually incorporated LCZ sub-classes to evaluate UHI impacts across socio-economic neighborhoods (López-Guerrero et al., 2024) and to assess both extreme heat and air pollution risks in residential areas (Steeneveld et al., 2018). Another study developed LCZ sub-classes to represent different land cover types for residential areas in arid regions (Eldesoky et al., 2022). Collectively, these studies illustrate the need for data-driven refinements that allow for systematic identification of residential typo-morphologies.

Besides LCZs, other efforts have sought to refine typo-morphologies for climate risk assessments using supervised learning. In the Netherlands, neighborhoods have been classified by historical building periods to assess climate stress (Kleerekoper et al., 2017; Kluck et al., 2023), with similar classification efforts applied in Germany (Iqbal et al., 2024; Klopfer, 2023). This approach leverages the fact that buildings from specific historical periods share construction methods, materials, and architectural styles, all of which influence thermal mass, ventilation patterns, and heat retention. However, while this historical categorization provides a practical starting point, it shares similar limitations as LCZs, as both are based on predetermined, expert-driven categories that assume homogeneity within groups. In reality, the built environment is highly heterogeneous, with neighborhoods often containing mixed building periods, varied construction qualities, and other modifications that do not conform to specific historical classification (Geiß et al., 2019). These predefined taxonomies may oversimplify complex urban fabrics and overlook emergent residential forms that do not fit established typologies. Unsupervised clustering offers a potential alternative by reducing expert bias and autonomously revealing unrecognized urban form patterns (Wang and Biljecki, 2022).

These challenges highlight the need for approaches that refine residential neighborhoods to be both globally comparable and contextually relevant. This paper therefore aims to refine representative residential typo-morphologies for enhanced urban heat vulnerability assessment using an unsupervised, data-driven approach. Furthermore, we pursue two interrelated objectives: (i) First, we identify which urban morphological and canopy parameters maximize separation between residential clusters while maintaining interpretability (Bishop & Nasrabadi, 2006). This involves exploring different parameter combinations to determine which parameter set most effectively distinguishes residential typo-morphologies. (ii) Second, we demonstrate the relevance of the derived residential typo-morphologies for urban heat vulnerability assessment. To achieve this, we pursue three complementary evaluations, where we compare the clustering results with standard LCZ parameters, verify against building construction distribution by historical period and secondary 3D sources (e.g., Google Earth and 3DBAG), and analyze UHI_{max} intensity patterns. Ultimately, this approach maintains the global comparability of LCZs while enhancing local relevance, providing researchers, urban planners and practitioners with a framework for advancing research and planning targeted climate adaptation interventions.

2. Methodology

2.1. Study area

In this study, we examined Dutch residential settlements with population densities exceeding 1,000 inhabitants per km^2. In total, the study area encompassed 99 Dutch cities (Fig. 1). The Netherlands has a temperate maritime climate, with cities characterized by compactness and relatively small land areas.

For the clustering analysis, the morphological and canopy parameters were aggregated into 100 m × 100 m grid cells provided by Statistics Netherlands (CBS) for 2023. The grid covers approximately 186,580 hectares in total and has been filtered to include only residential areas with at least five inhabitants, in line with CBS's privacy restrictions on smaller populations. The use of this grid offers three key advantages. First, it enables users to link socio-economic census data provided by CBS for future research extensions. Second, it ensures temporal consistency through fixed boundaries, unlike changing administrative boundaries. Third, it adopts the 100 m × 100 m resolution used in existing LCZ classifications, ensuring a consistent reference scale when comparing the clustering results.

Fig. 2 presents the methodological workflow adopted in this study. First, Principal Component Analysis was applied to identify the parameters that maximize variance and separation in the data space. Next, the Davis-Boudlin index, an internal clustering validation metric, was used to determine the optimal number of clusters (k) for the k-means algorithm. Finally, the clustering results were evaluated through three complementary approaches, which are described in detail in Section 2.5.

For reproducibility, all analyses were conducted using R (version 4.4.0) and Python, with all data, code, and analytical procedures fully documented and available at the 4TU.ResearchData repositiory.

2.2. Urban morphological and canopy parameters

Table 1 presents 17 parameters from the domains of urban planning and urban climatology that influence microclimates, as identified through theoretical and empirical studies. All mathematical formulas and data sources used for calculating the parameters are provided in Table A.2 in the appendix.

Building heights represent a key parameter regulating temperatures within urban canyons by affecting wind patterns, radiation exposure and heat absorption (Oke, 1978). During the night, tall buildings can influence urban temperatures in various ways. On one hand, they can contribute to warming by trapping radiation and facilitating the horizontal movement of warm air, known as advection, into cooler areas

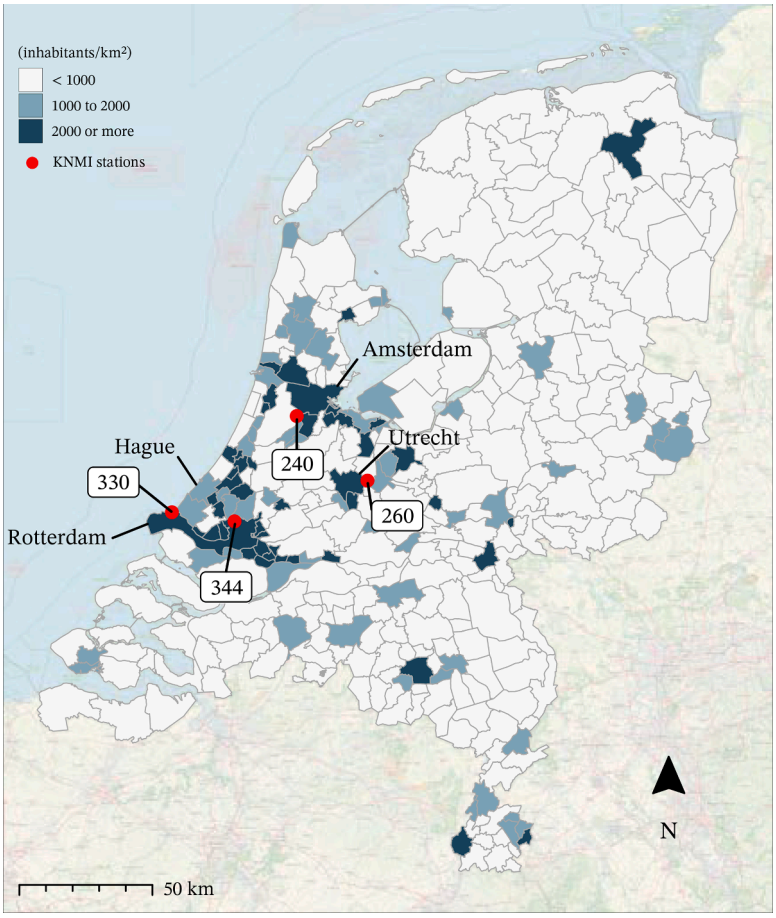

Fig. 1. Geographic locations of rural weather stations and Dutch municipalities with a population density ≥ 1000 inhabitants/km².

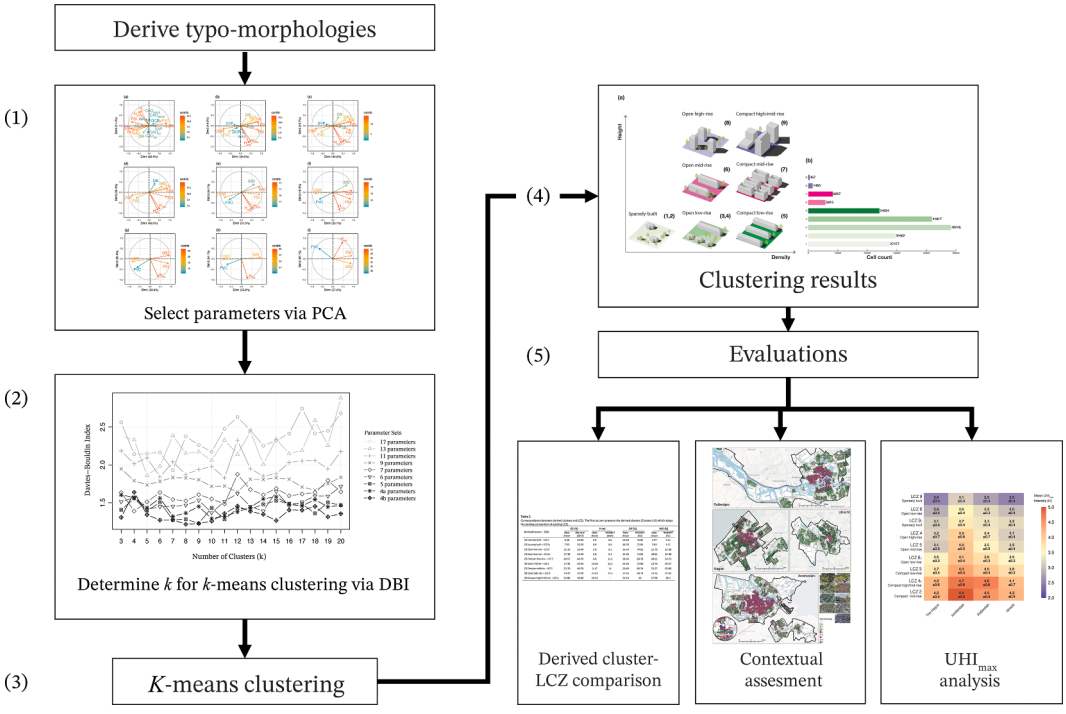

Fig. 2. Flowchart of the research methodology.

(Kolokotsa et al., 2022). On the other hand, tall buildings can promote cooling through vertical air mixing, as turbulence brings cooler air from

Table 1
Overview of parameters mediating microclimates.

Parameter	Abbreviation	Description	References
Building heights	H_{avg}	The average height of all buildings in a given area.	(Lin et al., 2023; Peeters and Etzion, 2012)
	H_{95th}	The 95th percentile height of all buildings in a given area.	(Oke et al., 2017)
Ground space index	GSI	The ratio of building footprint to plot area. This represents the horizontal density of development.	(Meiyan Zhao and Xu, 2016)
Floor space index	FSI	The building intensity ratio of total floor area to plot area. Higher values indicate more built floor space relative to land area.	(Maiullari et al., 2021; Wu et al., 2024)
Open space ratio	OSR	The ratio of open space to the areas of buildings on a site.	(Apreda et al., 2020; Boccalatte et al., 2023; Villaverde et al., 2024)
Street length	SL	The total length of streets in a given area.	(Guo et al., 2024; Wu et al., 2022)
Canyon axis orientation	CAO_{NS}	The proportion of street length oriented in a specfic direction (e.g., north-south, east-west) relative to the street length within a given site.	(Wu et al., 2022; Yin et al., 2019)
	CAO_{EW}		
	CAO_{NWSE}		
	CAO_{NESW}		
Frontal area index	FAI	The ratio of the total building surface area perpendicular to theoncoming wind direction to the plan area of a given site.	(Grimmond and Oke, 1999)
Minimum distance between buildings	DB	The average minimum distance between nearby buildings in a given area.	(Joshi et al., 2022)
Distance compactness ratio	DCR	The metric that quantifies the spatial distribution of buildings in a given area, serving as an indicator of urban compactness or sprawl; it measures the average distance between buildings relative to a reference point (i.e., centroid of a given site).	(Ma et al., 2021; Joshi et al., 2022)
Wall area index	WAI	The ratio of total exterior vertical wall surface area to total building footprint.	(Boccalatte et al., 2023; Sützl et al., 2024)
Sky view factor	SVF	The ratio of visible sky to the total hemisphere when viewed from a specific point on the ground.	(Dirksen et al., 2019; Middel et al., 2018).
Impervious surface density fraction	IMD	The fraction of the total site area that is covered by impervious surfaces (e.g., parking, roads, rooftops, etc.).	(Villaverde et al., 2024; Zhang et al., 2021)
Fractional vegetation cover	FVC	Proportion of ground surface covered by vegetation (tree canopy >2.5 m, shrubs, and low vegetation) relative to site area, excluding rooftop vegetation and agricultural land.	(Dirksen et al., 2019; Zhang et al., 2021)

higher altitudes to street level (Oke et al., 2017).

Also important are the floor space index (FSI), which reflects the vertical density of buildings, and the ground space index (GSI), which measures the horizontal coverage of buildings. Both FSI and GSI influence how much solar radiation penetrates into street canyons and open areas, thus affecting heat accumulation (Maiullari et al., 2021; Yang et al., 2013). Similarly, the open space ratio (OSR) represents the proportion of open spaces relative to built-up areas, where the size of open spaces affect heat absorption and solar gain (Kolokotsa et al., 2022; Villaverde et al., 2024).

Street length (SL) influences both airflow within urban canyons and serves as a proxy for vehicular traffic activity, with longer streets typically retaining more traffic and creating adverse thermal effects (Guo et al., 2024; Wu et al., 2022). Canyon axis orientation (CAO) affects air temperature by determining solar exposure on building facades, (Oke, 1997) and by blocking prevailing winds, and limiting natural cooling (Elbondira et al., 2021; Wu et al., 2022; Yin et al., 2019). Likewise, the frontal area index (FAI) measures how much building surface area is exposed to prevailing wind, another key factor in influencing airflow patterns (Grimmond and Oke, 1999).

The aspect ratio (H/W) represent the ratio of building height to street width and significantly influences several microclimate factors such as radiative exposure (Oke et al., 2017). However, we exclude it because street width is not trivial to estimate, particularly in open spaces, parks, and intersections where multiple interpretations are possible (Lindberg et al., 2015). To compensate for H/W, we incorporate proxy measures of area-wide compactness versus sprawl, including the average Euclidean distance from the block center to buildings (DCR) and the minimum distance to the nearest building (DB), which capture the spacing between buildings and the degree of contiguity within building blocks (Joshi et al., 2022). Additionally, we incorporate the wall area index (WAI), which quantifies building surfaces interacting with the ambient air and provides an alternative to H/W by representing vertical surfaces involved in radiation exchange and energy uptake (Boccalatte et al., 2023; Sützl et al., 2024).

Another significant parameter influencing urban microclimate is sky view factor (SVF), which measures the fraction of sky visible from street level and plays a critical role in modulating both incoming shortwave radiation and outgoing longwave radiation, thereby affecting surface heating and nocturnal cooling (Middel et al., 2018).

Lastly, both pervious and impervious surfaces influence urban hydrological processes by modifying the local surface energy balance. High impervious surface density (IMD) exacerbates urban heating by raising near-surface air temperatures, as impervious surfaces absorb solar radiation and release it primarily as sensible heat (Zhang et al., 2021). In contrast, fractional vegetation cover (FVC) mitigates heat accumulation by converting solar energy into latent heat through evapotranspiration and reducing incoming solar radiation through shading, thereby alleviating UHI effects (Dirksen et al., 2019; Zhang et al., 2021).

2.3. *Pre-processing for clustering*

Principal Component Analysis (PCA) is commonly used as a preprocessing step in clustering analyses (see e.g., Chen et al., 2022; Joshi et al., 2022; Villaverde et al., 2024), as it reduces data dimensionality by identifying key axes of variance (Ding and He, 2004). However, PCA was not used for clustering in this study, but rather for visualizing and transforming the data (i.e., 17 parameters listed in Table 1) into a space that revealed key structure through variance, thereby informing clustering. Furthermore, we used PCA biplots in our exploratory data analysis to understand which key parameters contributed the most to the overall variance structure and helped identify natural groupings in the data. Biplots provided a multivariate visualization approach that captured the joint contribution of all parameters in explaining the overall data structure, rather than examining individual pairwise relationships, and helped guide the selection of key parameters

for subsequent *k*-means clustering analysis.

For the pre-processing stage, all parameters were standardized using z-scores and cleaned for outliers prior to the analysis to avoid the variance of one parameter dominating the others (Tardioli et al., 2018; Gewers et al., 2021). We repeatedly refined the parameter selection using PCA biplots, removing those with low contributions (i.e., loading factors) and retained parameters that maximized the cumulative explained variance in the first two principal components, aiming for a threshold greater than 80%. However, the biplots served as a heuristic visualization tool to guide search, they alone cannot determine which parameter sets will yield well-separated clusters (Jolliffe and Cadima, 2016). Consequently, in Section 2.4., we employed an internal validation metric to objectively assess the clustering results of the various parameter sets explored through biplot analysis.

2.4. Clustering analysis

To perform the clustering analysis, we used the *k*-means clustering algorithm for its computational efficiency (Murphy, 2022), given the extensive geographic coverage and large volume of geospatial data involved in this study. Previous research have shown that *k*-means effectively identifies various typo-morphologies in urban areas (Joshi et al., 2022; Schirmer and Axhausen, 2019; Sützl et al., 2024; Villaverde et al., 2024; Wu et al., 2022). The algorithm partitioned the data into *k* non-overlapping clusters by minimizing the squared distances between data points and their centroids, thereby reducing intra-cluster variance and increasing inter-cluster separation (Murphy, 2022).

A prerequisite for *k*-means clustering is choosing a distance metric and selecting *k*. For this analysis, Euclidean distance was chosen as the distance metric. To guide the selection of *k*, we used the Davies-Bouldin Index (DBI), which evaluated the clustering quality by assessing both cluster compactness and separation. A lower DBI value indicated better separation between clusters and lower internal variance. By minimizing DBI, we found a *k* which maximizes separation while minimizing internal variance (Xiao et al., 2017).

2.5. Evaluation of clustering result

The clustering results were then evaluated through three complementary approaches: comparative, contextual, and UHI_{max} analysis.

2.5.1. Cluster-LCZ comparison

We selected the parameters H_{avg}, SVF, and IMD from the World Urban Database and Access Portal Tools (WUDAPT) LCZ dataset developed for the European domain (Demuzere et al., 2019) for the comparison against the derived clustering results. The H_{avg} values specifically reflect building height averages for Amsterdam, as these were the only city-level averages available in the dataset. In contrast, SVF and IMD values represent averages derived from selected European cities, consistent with the approach in Demuzere et al. (2019). We also incorporated the GSI, which is equivalent to the building plan fraction (λ_p) as specified in Oke et al.'s (2017) global lookup table.

2.5.2. Contextual assessment

To evaluate how well the clustering results reflect observable urban form types, we focused on four polycentric Dutch cities (Amsterdam, Rotterdam, Utrecht, and The Hague). The contextual assessment was carried out through secondary sources, including the 3D Registration of Buildings and Addresses (3DBAG) viewer and Google Earth. These cities represent a wide range of housing types that mirror broader residential trends across Northwest Europe (Dekker et al., 2012; Priemus, 2018). Additional contextual checks were performed by examining the distribution of construction building periods within each cluster, providing further objectivity to the evaluation process. In total, four historical periods were defined to capture key morphological transitions and policy interventions that shaped urban housing development: these are pre-war (< 1950), post-war (1950–1975), urban renewal (1975–1990), and VINEX (< 1990).

2.5.3. UHI_{max} analysis

We evaluated the UHI_{max} profiles of clustering results for the four major Dutch cities. To calculate UHI_{max}, we applied the semi-diagnostic equation proposed by Theeuwes et al. (2017). This equation estimates daily UHI_{max} occurrences at a high spatial resolution by combining rural hourly meteorological data, including diurnal temperature range (DTR), total solar irradiance (S), and average wind speed (U) from nearby weather stations (Fig. 1.), as well as urban parameters, specifically SVF and FVC. The UHI_{max} equation is expressed as follows:

$$UHI_{max} = (2 - SVF - FVC)\sqrt[4]{(DTR^3 \cdot S)/U} \quad (1)$$

For this study, we analyzed the 95th percentile UHI_{max} during the summer of 2022 (June to September), modeled at a spatial resolution of 5 m. The 95th percentile was calculated separately for each city, to represent extreme heat conditions. It is also important to note that UHI_{max} only occurs under favorable meteorological conditions (Theeuwes et al., 2017). This period included a nationwide heatwave from 9 to 16 August, as reported by Royal Netherlands Meteorological Institute (KNMI). For further details on how the modeled UHI_{max} was operationalized and access to the dataset, readers can refer to Habib et al. (2025).

3. Results

In this section, we present the results of the unsupervised clustering analysis applied to residential neighborhoods across 99 highly urbanized Dutch cities. We first report the optimal parameter set selection and cluster configuration. We then characterize the clustering results (i.e. typo-morphologies) and evaluate their compatibility with existing LCZs, their contextual validity, and their relationship with UHI_{max} intensity.

3.1. Exploratory data analysis

In Fig. 3., the biplots reveal how removing low-contribution parameters increases the cumulative explained variance of the first two dimensions of the PCA. Starting with all 17 parameters (panel a), the first two dimensions explained only approximately 38% of the total variance, potentially indicating redundancy and noise among these parameters based on their directional similarities and varying contribution.

Most of the improvement in cumulative explained variance occurred after removing the parameters related to canyon axis orientation (CAO_{NS}, CAO_{EW}, CAO_{NWSE}, and CAO_{NESW}). A previous study on detecting urban morphological patterns have shown that canyon orientation often shows no clear influence in their classification models, whereas factors such as average building height, density, and the number of building blocks contribute more effectively (Taubenböck et al., 2018).

As other low-contribution parameters were progressively removed, the cumulative explained variance increased to over 80% in panels (g), (h), and (i). Since biplots provide only a heuristic visualization of clustering patterns, DBI analysis was used to quantitatively evaluate cluster separation.

3.2. Number of clusters

To guide the selection of *k*, we evaluated each parameter set using the DBI (Fig. 4). The plot in Fig. 4 reveals that both the 5 and 4b parameter sets (panels g and i) achieved the lowest DBI scores, on average. The 4b parameter set shows a notable minimum at $k = 8$, while the 5 parameter set reaches its lowest point at $k = 9$. Based on these findings, we proceeded to evaluate the clustering results for $k = 8$ (4b parameters) and $k = 9$ (5 parameters). The 5 parameter set showed the

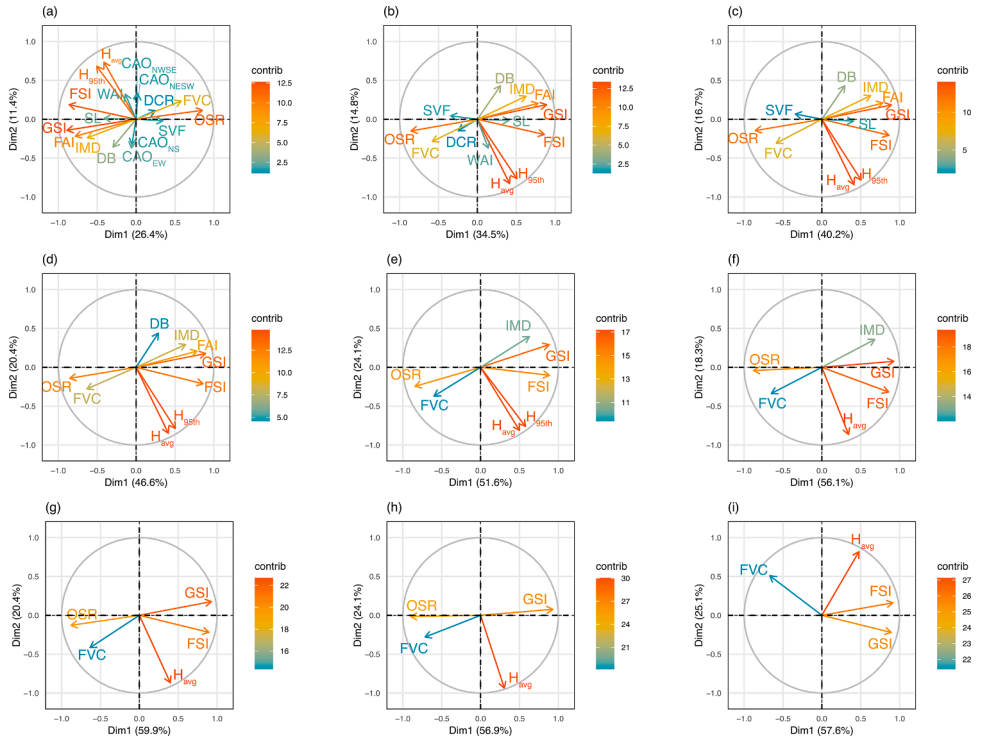

Fig. 3. PCA biplots: (a) 17 parameters, (b) 13 parameters, (c) 11 parameters, (d) 9 parameters, (e) 7 parameters, (f) 6 parameters, (g) 5 parameters, (h) 4a parameters, and (i) 4b parameters. Vectors represent the loadings of each parameter on the first two principal components, with color intensity indicating their contribution.

closets alignment with parameters of the established LCZ categories. In contrast, the 4b parameter set generated numerous variations of low-rise LCZs and lead to mid- and high-rise types to be grouped together, reducing their distinguishability (see Table A.3 in the appendix).

3.3. Clustering results

Applying *k*-means clustering to five parameter sets (FSI, GSI, OSR, H_{avg}, and FVC) produced nine distinct residential typo-morphologies relatable to existing LCZs. Table 2 and Fig. 5 presents the morphological and canopy characteristics of each cluster, while Fig. 6 and Fig. 7 provide schematic representations, spatial distributions, and grid cell counts. The derived clusters align with six established LCZ types while revealing sub-classes not captured by the standard framework. Below we characterize each cluster according to its morphological and canopy parameters, as well as its correspondence to LCZ types:

- **Cluster 1** (LCZ 9 — sparsely built): Features detached housing with the highest vegetation coverage (FVC ~ 70%), low building coverage (GSI ~ 15%), and low-rise structures (< 3 stories). This cluster exhibits the lowest mean UHI_{max} intensity (2.8 K) and is predominantly located nearby suburban peripheries.
- **Cluster 2** (LCZ 9_D — sparsely built, low vegetation variant): Encompasses a variant within the sparsely built category, the 'D' subscript indicates higher sealed surface coverage (IMD ~ 35% compared to ~ 20% in Cluster 1), reduced FVC and tree coverage (< 25%), but similar building heights and footprint.
- **Cluster 3** (LCZ 6 — open low-rise): Comprises largely of semi-detached houses with moderate vegetation coverage (FVC ~ 50%). Buildings remain low-rise (< 3 stories) with moderate building coverage (GSI ~ 30%).
- **Cluster 4** (LCZ 6_D — open low-rise, low vegetation variant): Represents a less vegetated variant of open low-rise housing, featuring

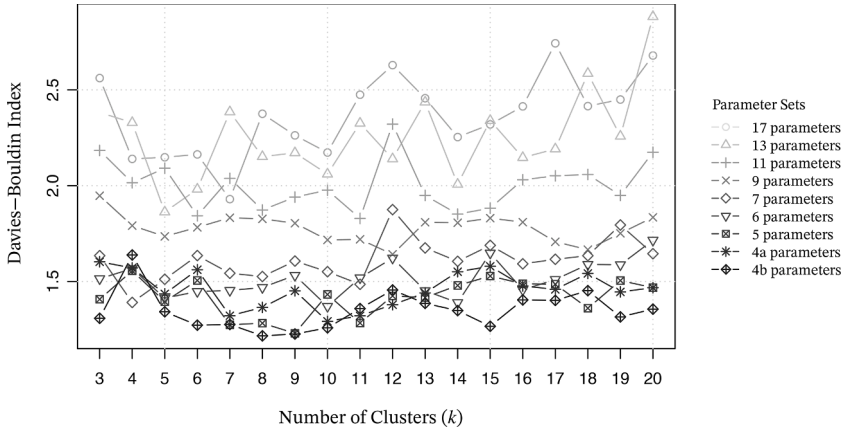

Fig. 4. DBI scores across different numbers of clusters (*k*) for six parameter sets.

Table 2
Correspondence between derived clusters and LCZs. The first column presents the derived clusters (Clusters 1-9) which adopt the naming convention of existing LCZs.

Derived clusters – LCZs	GSI (%)		H (m)		SVF (%)		IMD (%)	
	Data-driven	Oke et al. (2017)	Data-driven	WUDAPT (AMS)	Data-driven	WUDAPT (EU)	Data-driven	WUDAPT (EU)
(1) Sparsely built — LCZ 9	6–18	10–20	6–9	8.6	32–60	72–85	1–47	5–21
(2) Sparsely built — LCZ 9_D	7–23	10–20	6–9	8.6	46–70	72–85	7–63	5–21
(3) Open low-rise — LCZ 6	21–33	20–40	5–8	8.2	36–54	74–82	25–70	15–38
(4) Open low-rise — LCZ 6_D	27–38	20–40	5–8	8.2	42–56	74–82	38–82	15–38
(5) Compact low-rise — LCZ 3	40–57	40–70	6–9	11.1	38–54	68–79	48–91	52–73
(6) Open midrise — LCZ 5	17–38	20–40	13–20	12.1	32–56	72–80	23–76	34–57
(7) Compact midrise — LCZ 2	53–79	40–70	9–17	14	29–49	66–74	55–97	63–80
(8) Open high-rise — LCZ 4	10–40	20–40	25–44	12.5	32–56	60–79	23–76	37–43
(9) Compact high/mid-rise — LCZ 4_2	54–86	40–60	16–45	–	31–54	63	37–98	91

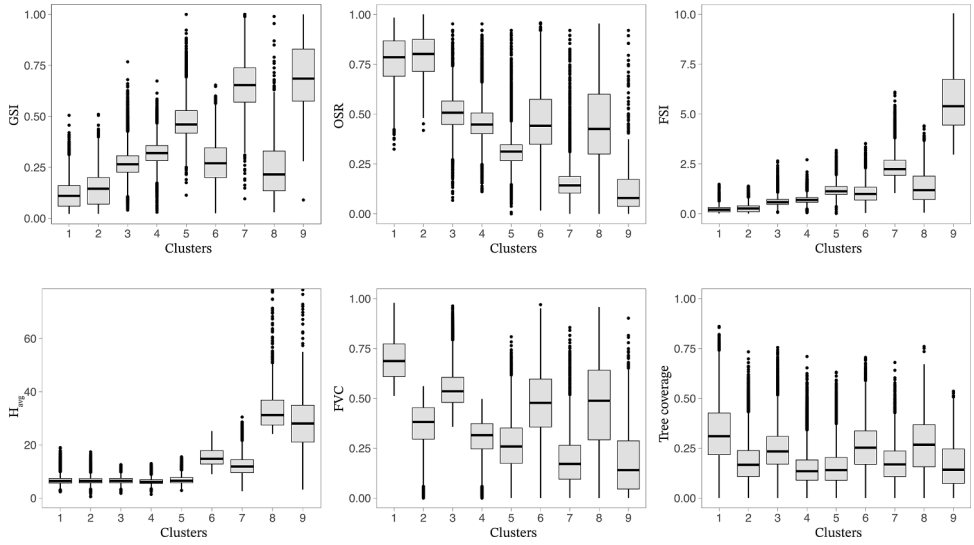

Fig. 5. Distribution of morphological and canopy parameters of Cluster (1–9). Outliers beyond the displayed y-axis range are not shown for visual clarity. Tree coverage is one of three vegetation types that make up FVC along with shrubs and grass coverage.

similar building heights (< 3 stories) but significantly lower green space (FVC ~ 30%) and reduced tree coverage compared to Cluster 3. Together, Clusters 3–4 comprise the most extensive spatial coverage in Dutch residential areas.

- **Cluster 5** (LCZ 3 — compact low-rise): Contains compact row housing arranged in dense linear configurations with small private gardens. Buildings maintain similar heights to Clusters 1–4 (< 3 stories), but have considerably denser building footprints (GSI ~ 45%) and more impervious surfaces (48–91%) compared to Clusters 1–4.
- **Cluster 6** (LCZ 5 — open mid-rise): Consists of open mid-rise building arrangements with moderate vegetation cover (FVC ~ 40%), lower building coverage (GSI ~ 30%) with taller building structures (5 stories) compared to Cluster 5.
- **Cluster 7** (LCZ 2 — compact mid-rise): Reflects compact mid-rise developments that are predominantly located in city cores. The building stock consists largely of historical buildings (< 1950), averaging four stories and often forming courtyard-like configurations with little space for greenery and trees. It exhibits the highest mean UHI_{max} intensity (4.5 K).
- **Cluster 8** (LCZ 4 — open high-rise): Corresponds to open, high-rise areas where approximately half of the building stock consists of post-war structures built between 1950 and 1975. Typically located at the peripheries of city centers and features taller building structures (6–8 stories) with moderate building coverage (GSI ~ 25%).
- **Cluster 9** (LCZ 4_2 — compact high/mid-rise): Exhibits the highest building coverage (GSI ~ 70%) and extensive surface sealing. The mix of pre-war and post-war buildings indicates urban infill in city cores, where modern high-rise buildings are situated adjacent to compact mid-rise fabric (LCZ 2).

3.4. Evaluation of residential typo-morphologies

3.4.1. LCZs comparison

The derived clusters show varying degrees of correspondence with established LCZ categories (Table 2). Parameter-by-parameter analysis reveals at times patterns of strong alignment and systematic deviation. GSI values demonstrate strong correspondence, consistently aligning with Oke et al. (2017) ranges across most cluster types. However, systematic deviations emerged in other parameters.

H_{avg} values show relatively strong alignment with WUDAPT references for lower-rise classes, while values for mid- and high-rise clusters are marginally higher, particularly in the high-rise category. For example, open high-rise clusters (Cluster 8) yield 25–44 m compared to WUDAPT's 12.5 m. As shown in Fig. 6, the clustering approach in this study is particularly effective at identifying high-rise urban forms that are underrepresented in existing EU WUDAPT data (see Table A.1 in the appendix). Similarly, IMD values are systematically higher across all derived clusters, particularly pronounced in compact developments where values reach 48–97% compared to WUDAPT's estimates. Both deviations of H_{avg} and IMD may reflect the contextual traits of Dutch residential environment compared to other European cities considered in the WUDAPT's dataset.

Meanwhile, SVF values of the derived clusters are systematically

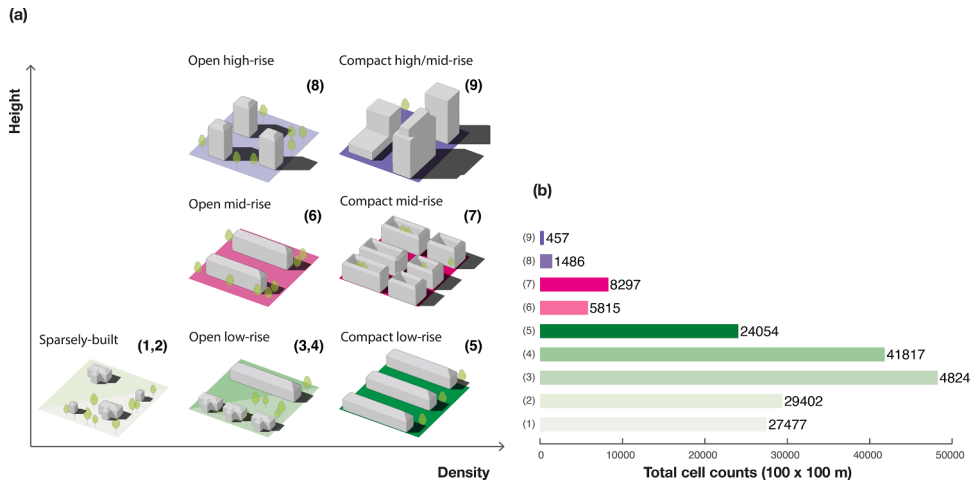

Fig. 6. Schematic illustration showing (a) the distribution of the residential typo-morphologies arranged relative to its relationship between height and density; (b) the total distribution of residential typo-morphologies grid cells across the geographic study area as shown in Fig. 1.

Table 3
Distribution of residential LCZ types in the Netherlands by building construction period, showing the percentage of buildings in each 100 m × 100 m grid cell corresponding to their predominant historical periods.

Clusters—LCZs	Pre-war (< 1950)	Post-war (1950–1975)	Urban renewal (1975–1990)	VINEX (> 1990)
(1) — LCZ 9	22.0	24.7	17.4	36.0
(2) — LCZ 9_D	18.5	21.9	16.8	42.8
(3) — LCZ 6	13.9	30.6	25.0	30.6
(4) — LCZ 6_D	13.0	30.3	20.8	35.9
(5) — LCZ 3	31.1	20.2	16.9	31.8
(6) — LCZ 5	13.4	38.8	12.7	35.2
(7) — LCZ 2	53.2	10.7	11.7	24.4
(8) — LCZ 4	1.4	49.7	9.78	39.1
(9) — LCZ 4_2	10.8	23.1	13.9	52.2

lower and more variable (29–70%) than WUDAPT's constrained ranges (60−85%) across all LCZs. The SVF differences may stem from the higher spatial resolution DSM datasets used in this study compared to the coarser resolution methods underlying WUDAPT classifications, where SVF values are constrained to street-level perspectives and do not include SVF values from spaces such as courtyards, parks, and private gardens.

3.4.2. *Contextual evaluation*

The numerical and geographical distribution of the derived clusters (i.e., typo-morphologies) across the Netherlands, as shown in Fig. 5, along with the summaries of the building stock by construction period outlined in Table 3 and morphological and canopy parameter characteristics (Table 2 and Fig. 3), guided expert assessments during the second phase of evaluation.

The spatial distribution of the nine identified clusters across the Netherlands reveals varying patterns that reflect the country's historical urban development. Sparse and open low-rise categories dominate the clustering results, collectively representing approximately 79% of all grid cells and demonstrating the typically dispersed, low-density nature of Dutch residential developments.

- *Low-rise and suburban transition (Cluster 1-4)*

The prevalence of Clusters 1–4 (LCZ 6 and LCZ 9) increased substantially from 13–22% of the land area in 1950 to 30–43% in recent decades. This expansion reflects the gradual growth of low-density developments outside urban cores, which aligns with urban sprawl patterns. Table 3 shows a temporary deceleration in this expansion between 1975 and 1990, which aligns with documented Dutch policy initiatives aimed at limiting urban sprawl during this period (Bontje, 2005).

Overall, Clusters 1–4 exhibit subtle morphological differences among themselves. Clusters 1–2 are characterized by extremely low building coverage (GSI < 0.23) and high open space ratios (OSR ~ 0.8). Meanwhile, Clusters 3–4 maintain the low-rise character while increasing built-up density (GSI ~ 0.3). Within these pairs, Cluster 2 differs from Cluster 1, and similarly, Cluster 4 differs from Cluster 3, primarily in land cover characteristics (FVC and IMD) rather than building density or height.

Cluster 5 represents the more compact end of low-rise development with dense row housing with small private gardens.

- *Mid- and high-rise urban areas (Cluster 5–9)*

Mid-rise morphologies (Clusters 6–7) account for less than 8% of the urban fabric in this study, though their spatial concentration in major polycentric urban centers makes them appear more prominent in Fig. 7. Moreover, spatial distribution of Cluster 7 is largely within the historical city cores, where most of the building stocks were constructed before 1950 (Table 3). These mid-rise historical areas, such as Amsterdam's neighborhoods adjacent to the canal districts, are characterized by distinctive courtyard configurations and narrow street canyons. Meanwhile, high-rise morphologies, like Cluster 8, predominantly represent post-war housing estates (1950–1975) at the city peripheries, while Cluster 9 is concentrated in urban cores, particularly evident in Rotterdam's reconstructed center, where more than half of the buildings are contemporary high-density developments blending compact mid-rise and high-rise characteristics.

3.4.3. *UHI_{max} analysis*

Fig. 8 shows the gradients of UHI_{max} intensities in all residential typo-morphologies, with differences of 1.7 ± 0.4 K between sparsely

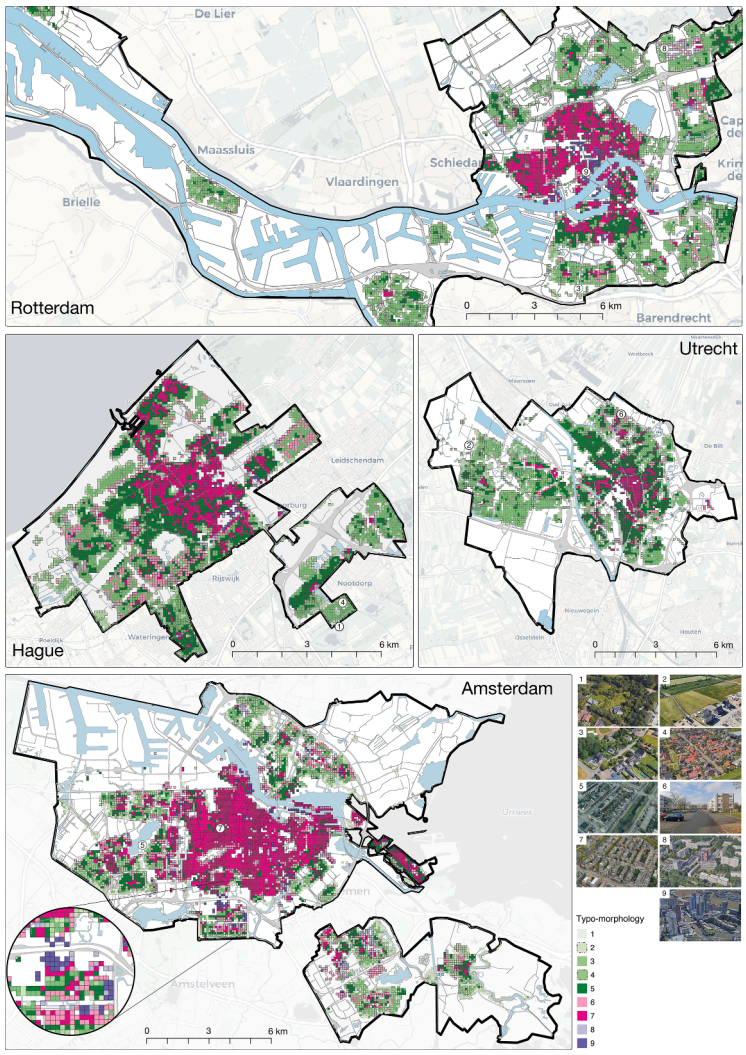

Fig. 7. Geographical distribution of the classification in Amsterdam, Rotterdam, Utrecht, and The Hague. Empirical examples (bottom-right) of the residential typo-morphologies found in the Dutch urban landscape; source: Google Earth, © Google LLC, 2025.

built and compact areas in the four analyzed cities. Table A.1 in the appendix shows that the WUDAPT LCZ classification identifies only 930 ha of compact mid-rise (LCZ 2) across the entire Netherlands, whereas our approach detects 8,279 ha within the 99 Dutch cities alone. Similarly, open mid-rise (LCZ 5) and open high-rise (LCZ 4) types are nearly absent from WUDAPT dataset, yet they collectively account for 9% of the total grid cells. Without this refined mapping, the range of UHI_{max} range would not be unobserved, as these typo-morphologies would be erroneously aggregated into other LCZ types. Importantly, WUDAPT LCZ classifications in the Netherlands underrepresent the densest morphological types (LCZ 2 and LCZ 4_2), which means overlooking neighborhoods that experience the highest heat exposure.

Across all four cities, consistent UHI_{max} patterns emerge with respect to density, height, and land cover. Sparsely built areas (LCZ 9) consistently show the lowest intensities (2.5–3.1 K), while compact mid- and high-rise areas (LCZ 2 and LCZ 4_2) exhibit the highest UHI_{max} (4.1–4.9 K) intensities. As expected, between LCZ 9 and the densest types, increasing density corresponds to a reduction in green coverage. FVC decreases from 70% in LCZ 9 to 15% in LCZ 2, while IMD shows the opposite trend, increasing from approximately 25% to 70%. Similarly, building footprints (i.e., GSI) increases from 12% in sparse types to 65–70% in compact ones (Fig. 5, Table 2), illustrating how built-up areas replace vegetated surfaces as density increases. The identified subclasses (LCZ 6_D and LCZ 9_D) also exhbit distinct UHI_{max} intensities compared to their respective base types (LCZ 6 and LCZ 9). Despite having similar H_{avg} and GSI values, LCZ 9_D and LCZ 6_D exhibit higher UHI_{max} intensities than their non-D counterparts, which is higher by 0.5–0.7 K and 0.5–0.6 K, respectively. These differences also correspond to approximately 15% and 25% lower FVC in the D-variants of LCZ 9 and LCZ 6, respectively. Notably, LCZ 6_D reaches UHI_{max} intensities (3.5–4.1 K) similar to open high-rise types (3.1–3.9 K), despite its substantially lower average building height (H_{avg} 5–8 m).

Remarkably, tree cover across all typo-morphologies ranges from 15% to 30%, but most typologies are below 15%. Open mid-rise and high-rise types (LCZ 4–5) have the highest vegetation coverage after LCZ 9. The strongest contrast occurs between LCZ 9 and LCZ 4_2, where vegetation cover differs by roughly 50%. This highlights substantial opportunities to expand tree cover in residential areas (especially low-rise areas) to help reduce heat exposure.

4. Discussion and conclusions

Motivated by the limitations of existing urban morphological classifications, such as LCZs and other supervised classifications based on historical building period, this study developed an unsupervised, data-driven approach to refine residential typo-morphologies for the Dutch context. Our results demonstrate that our approach can preserve the global comparability of LCZs while improving representation of urban

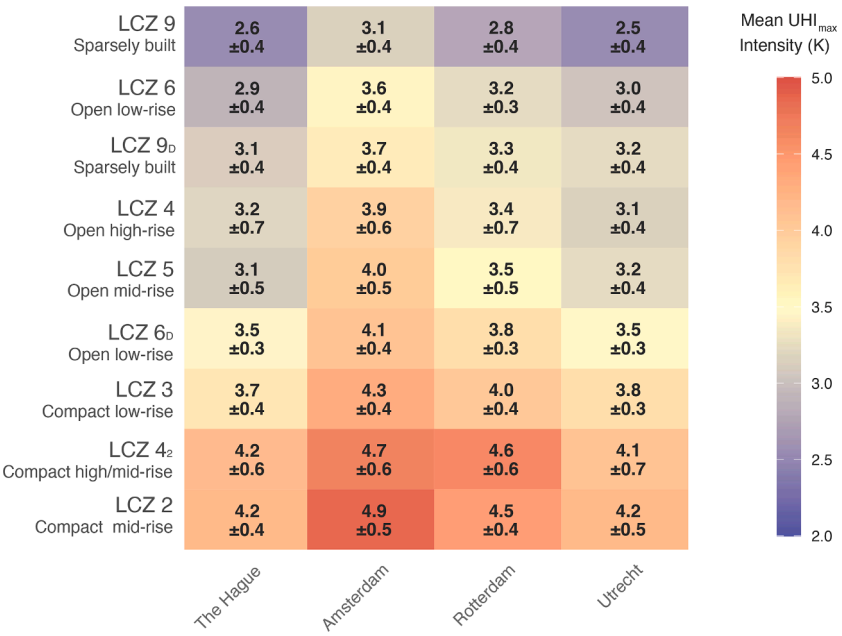

Fig. 8. Mean UHI_{max} intensity (K) of derived clusters across the four largest Dutch cities. Values represent air temperature differences relative to baseline conditions.

diversity within residential settlements. Below, we discuss our findings in relation to the two research objectives, followed by practical implications, study limitations, and future research directions.

4.1. Parameters selection for residential typo-morphologies

The first key finding of this study is that PCA reveals five parameters (GSI, FSI, OSR, H_{avg} and FVC), account for most explained cumulative variance (80%) across all parameters sets evaluated. Together, these five parameters capture the key aspects of urban morphology and canopy (density, height, spacing, and vegetation), features that LCZ classification similarly relies on. Notably, FSI, GSI, OSR, and H_{avg} are all needed to represent urban morphological characteristics, despite being strongly correlated. Urban morphology research shows that these density-related parameters, along with average building height, form a distinctive 'spatial fingerprint' reflecting specific urban forms (Pont and Haupt, 2023). Considering density parameters in isolation can be misleading. For instance, the same FSI value may correspond to either low-rise buildings covering entire plots or high-rise towers on small footprints (Pont and Haupt, 2023).

These results suggest that morphological parameters rooted in urban planning practice may capture LCZ characteristics more effectively than some traditional urban canopy parameters, at the given 100 m × 100 m spatial resolution examined in this study. Traditional parameters like SVF, while climatically relevant, may introduce noise when characterizing morphological form since they integrate both built structures and vegetation canopy. The practical significance of these morphological parameters is further supported by studies demonstrating their measurable impacts on building energy demands (Dab'at and Alqadi, 2024; Liu et al., 2025) and pedestrian-level microclimate during hot summers (Zhang et al., 2022). Ultimately, the benefit of these five parameters lies in their familiarity to urban planners and practitioners, facilitating integration into climate adaptation planning workflows.

4.2. Refined residential typo-morphologies and UHI_{max} patterns

Another key finding is that our data-driven approach identified nine residential LCZ types, improving the detection of underrepresented categories (LCZ 2, LCZ 4, LCZ 5) while revealing new sub-classes (LCZ 6_D, LCZ 9_D, and LCZ 4_2) not captured by standard LCZ classifications. Across the four cities, the absolute UHI_{max} differences (1.7 ± 0.4 K) occur between the densest urban cores (LCZ 4_2 and LCZ 2) and sparsely built areas (LCZ 9). Furthermore, the modeled UHI_{max} intensities in our study likely underestimate the total air temperature differences, especially for compact typo-morphologies. This underestimation likely stems from Eq. (1) not accounting for additional heat contributions from anthropogenic sources (e.g., traffic and building energy use) that typically characterize compact city centers (Javadpoor et al., 2024).

LCZ 4_2 largely represents recent dense high-rise developments that have emerged since the 1990s as part of urban densification and infill projects in existing urban Dutch fabric (Nabielek, 2012). Although LCZ 4_2 covers less than 1% of the study area, its detection is noteworthy, because both LCZ 4_2 and compact midrise areas (LCZ 2) experience the highest UHI_{max} intensities (4.1–4.7 K), making them priority targets for heat adaptation interventions. Previous research shows that dense, poorly ventilated urban areas are associated with elevated rates of cardiovascular-related emergency calls during heatwaves, particularly in socially deprived neighborhoods (Zendeli et al., 2025).

Another aspect to consider is the contribution of UHI to indoor overheating. While open high-rise areas (LCZ 4) areas do not exhibit high UHI_{max} compared to denser neighborhoods, their open urban form and the predominance of post-war dwellings make them vulnerable to heat exposure. Most of the Dutch post-war buildings lack mechanical ventilation, and without adequate solar protection, they are increasingly susceptible to indoor overheating (Hamdy et al., 2017). In our analysis, we observe that roughly half of the LCZ 4 dwellings date from the post-war period (1950–1975). Without refined identification of these residential typo-morphologies, vulnerability assessments risk underestimating high-exposure areas, potentially overlooking neighborhoods where residents face significant heat stress.

4.3. Implications for climate adaptation planning

The refined typo-morphologies offer actionable frameworks for designing context-appropriate adaptation strategies that can guide both research and urban planning efforts. Studies in other European cities demonstrate that compact mid-rise areas (LCZ 2) exhibit the highest day- and nighttime land surface temperatures (Wu et al., 2022). In the Netherlands, most LCZ 2 buildings predate the 1950s, and their architectural heritage, combined with limited space, calls for

context-sensitive interventions such as cool roofing, courtyard greening, and green façade (Sützl et al., 2024).

Across many low-rise and compact typo-morphologies, tree cover is less than 25%, reflecting a general lack of shade and limited protection from heat exposure caused by direct solar radiation. Open low-rise developments, particularly LCZ 3 and LCZ 6_D, provide greater opportunities for street tree planting, as they offer more space to replace paved surfaces with greenery. Recently, several Dutch authorities have been addressing the high prevalence of paved surfaces through programs encouraging citizen-led initiatives (tegelwippen), in which residents participate by removing tiles in their neighborhoods (ANP, 2024). Integrating typo-morphological mapping could enable more strategic prioritization and monitoring of greening interventions by directing resources to areas with the highest heat exposure.

4.4. Limitations

There are inherent methodological limitations that warrant consideration. First, a notable limitation of this study lies in its reliance on the 100 m × 100 m grid cell resolution provided by CBS, which may introduce biases related to the modifiable areal unit problem (Openshaw, 1984). Using a single spatial resolution can artificially segment continuous urban patterns, potentially affecting the interpretation of spatial relationships. Although the 100 m × 100 m grid represents the finest publicly available spatial resolution from CBS, our analysis indicates that high-rise developments comprise only about 1% of all grid cells. This highlights the need for finer-scale data to capture such sparse morphological structures (Ullmann et al., 2022; Yu et al., 2023). While testing other grid sizes would be ideal, the alternative 500 m × 500 m grid cells from CBS is too coarse for the purposes of this analysis. Nevertheless, a key advantage of using the 100 m × 100 m grid lies in its compatibility with official socio-demographic data, supporting future research aimed at advancing climate adaptation strategies.

A second limitation relates to UHI_{max} estimation. Because ground-truth measurements are not feasible given the geographic extent of this study, Eq. (1) approach is used instead. Notably, Eq. (1) has acknowledged limitations, as it does not solve the full set of physical equations governing heat transfer, energy balance, or fluid dynamics. It also does not account for anthropogenic heat and assumes uniform building materials which is an assumption that does not hold. Nevertheless, Eq. (1) has been extensively validated in previous research (Dirksen et al., 2019; Habib et al., 2025; Koopmans et al., 2020; Theeuwes et al., 2017; Zhang et al., 2019), with reported RMSE values ranging from 0.9 K to 1.29 K.

4.5. Future research direction

Several promising research avenues emerge from this work. First, the typo-morphological refinements identified for the Dutch residential context can be used to facilitate comparability across other Northwest European cities with similar urbanization developments. Second, future studies can test the transferability of the parameter set and clustering methodology while potentially identifying region-specific morphological patterns relevant for climate adaptation. Third, integration with socio-economic and environmental datasets could explore relationships between detected morphological clusters and demographic characteristics, building on the method's compatibility with CBS grid data to inform equity-conscious climate adaptation strategies. Such integration would transform the morphological exposure framework developed here into a comprehensive vulnerability assessment tool, enabling researchers, urban planners and practitioners to identify areas where heat is most intense and where it poses the greatest risk to human health and wellbeing.

Ethics statement

The authors have read and comply with the ethical requirements for publication in Sustainable Cities and Societies. The authors also confirm that this work does not involve human subjects, animal experiments, or any data collected from social media platforms.

CRediT authorship contribution statement

Maha Habib: Writing – original draft, Visualization, Validation, Methodology, Investigation, Formal analysis, Data curation, Conceptualization. **Doruntina Zendeli:** Writing – review & editing, Investigation. **Marjolein van Esch:** Writing – review & editing, Supervision. **Wim J. Timmermans:** Writing – review & editing, Supervision, Conceptualization. **Maarten van Ham:** Writing – review & editing, Supervision, Project administration.

Declaration of competing interest

The authors declare that they have no known competing financial interests or personal relationships that could have appeared to influence the work reported in this paper.

Acknowledgements

This research was conducted as part of Frontrunner 4 project within the Pandemic and Disaster Preparedness Center (PDPC), Delft, Rotterdam, the Netherlands.

Appendix

Table A.1
Distribution of LCZ counts and corresponding surface areas (ha) across the Netherlands, based on 100 m × 100 m grid cells from WUDAPT. Only LCZs relevant to residential and urban built environment are considered in this study. LCZ 7 (lightweight low-rise), LCZ 8 (large low-rise), and LCZ 10 (heavy industry), typically associated with industrial or atypical European domains, are excluded.

LCZ 1 — Compact high-rise	LCZ 2 — Compact mid-rise	LCZ 3 — Compact low-rise	LCZ 4 — Open high-rise	LCZ 5 — Open mid-rise	LCZ 6 — Open low-rise	LCZ 9 — Sparsely built
0	930	3296	0	96	138699	1457

Table A.2
All mathematical formulas are specific to one 100 m × 100 m grid cell. All datasets are sourced from publicly available secondary sources or derived therefrom.

Mathematical formula	Source	Specification parameters
$H_{avg} = (1/n)\cdot\sum_{i=1}^{n}\lvert H_{max,i} - H_{min,i}\rvert$	3DBAG (2022)	*Average building height: where $H_{max,i}$ and $H_{min,i}$ denotes the maximum and minimum heights for each building i, respectively and n is the total number of buildings.*
$H_{95} = P_{95}(\lvert H_{max,\,i} - H_{min,\,i}\rvert : i = 1, 2, \ldots, n)$	3DBAG (2022)	*The 95th percentile of building heights: where n is the total number of buildings, and $H_{max,i}$ and $H_{min,i}$ denotes the maximum and minimum heights, for building i, respectively.*
$GSI = (1/n)\cdot\sum_{i=1}^{n} A_i/A_{lot,i}$	Rudifun (2022)	*Ground Space Index: where n is the total number of building blocks, A_i is the footprint of the building block i, and $A_{lot,\,i}$ is the total site area of building i.*
$FSI = (1/n)\cdot\sum_{i=1}^{n} F_i/A_i$	Rudifun (2022)	*Floor Space Index: where n is the total number of building blocks, F_i is the total floor area of building block i (across all floors), and A_i is the footprint of the building i.*
$OSR = (1/n)\cdot\sum_{i=1}^{n}(1 - (A_i/A_{lot,i})) - (F_i/A_i)$	Rudifun (2022)	*Open Space Ratio: where n is the total number of building blocks, $1-(A_i/A_{lot,i})$ denotes the unbuilt space of building block i and F_i/A_i is the floor area ratio of building block i. Note that the two expressions are constructed using the GSI and FSI, as described above.*
$SL = (1/n)\cdot\sum_{i=1}^{n} SL_i$	Derived from Land Registry and Public Registers Service (2025)	*Street Length: where SL_i represents the length of street i, and n is the total number of streets.*
$CAO_{dir} = (1/SL)\cdot\sum_{i=1}^{n}(SL_{dir,i})$	Derived from Land Registry and Public Registers Service (2025)	*Canyon Axis Orientation: where n is the total number of streets in a given direction dir, $SL_{dir,i}$ represents the street length in a direction dir classified by 45-degree azimuth angle range (i.e, NS, EW, NESW, or NWSE), for a street i, and SL is the sum of all street lengths.*
$FAI = (1/n)\cdot(\sum_{i=1}^{n} A_{proj,i})/A$	Derived from 3DBAG (2022)	*Frontal Area Index: where n is the total number of buildings, $A_{proj,i}$ is total area of each building i facet projected onto the plane normal to the incoming wind direction and A is the total site area.*
$WAI = (1/n)\cdot\sum_{i=1}^{n}(V_i/A_i)$	3DBAG (2022)	*Wall Area Index: where V_i is the total exterior vertical surface area of each building i, A_i is the footprint of the building, and n is the total number of buildings.*
$DB = (1/n)\cdot\sum_{i=1}^{n}\underset{j\neq i}{mind}(B_i, B_j)$	Derived from 3DBAG (2022)	*Minimum distance between buildings: where n is the total number of buildings, $d(B_i, B_j)$ is the Euclidean distance between the buildings B_i, B_j.*
$DCR = (1/n)\cdot\sum_{i=1}^{n} d(C, B_i)$	Derived from 3DBAG (2022)	*Distance Compactness Ratio: where n is the total number of buildings, $d(C, B_i)$ is the 2D Euclidean distance from the centroid of the grid cell to the centroid of building i.*
SVF	Habib et al. (2025)	*Sky View Factor: readers can refer to Habib et al. (2025) to obtain mathematical formulas and parameters used to operationalize the SVF calculation.*
$IMD = (1/n)\cdot\sum_{i=1}^{n} IMD_i$	Derived from Copernicus Land Monitoring Service (2018)	*Impervious Surface Density Fraction: where n is the total number of grid cells, and IMD_i is the impervious surface density (0-1) for each grid cell i.*
$FVC = (1/n)\cdot\sum_{i=1}^{n}(T_i + G_i + S_i)$	Derived from RIVM (2022)	*Fractional Vegetational Cover: where n is the total number of grid cells, T_i is the tree cover fraction (0-1), $G_i$is the grass cover fraction (0-1), and S_i is the shrub cover fraction (0-1) for each grid cell i, and together they do not exceed a value of 1.*

Table A.3
Summary of 4b parameters.

Derived clusters	GSI (%)	H_{avg} (m)	SVF (%)	IMD (%)
(1)	6–18	6–9	32–60	1–47
(2)	7–23	6–9	46–70	7–63
(3)	21–33	5–8	36–54	25–70
(4)	27–38	5–8	42–56	38–82
(5)	40–57	6–9	38–54	48–91
(6)	17–38	13–20	32–56	23–76
(7)	53–79	9–17	29–49	55–97
(8)	10–40	25–44	32–56	23–76

Data availability

The data that support the findings of this study are openly available in the 4TU.ResearchData repository.

Clustering Approach to Residential Typo-morphologies Across Multiple Dutch Cities for Urban Heat Vulnerability Assessment (Original data) (4TU.ResearchData)

References

Alexander, P. J., & Mills, G. (2014). Local climate classification and Dublin's urban heat island. *Atmosphere, 5*(4), 755–774. https://doi.org/10.3390/atmos5040755

ANP. (2024). *100 voetbalvelden aan groen erbij na NK Tegelwippen: Nederland verbreekt opnieuw records*. https://persportaal.anp.nl/artikel/ad837dcd-4765-4e6a-908a-daa582ef4d3c/100-voetbalvelden-aan-groen-erbij-na-nk-tegelwippen-nederland-verbreekt-opnieuw-records.

Apreda, C., Reder, A., & Mercogliano, P. (2020). Urban morphology parameterization for assessing the effects of housing blocks layouts on air temperature in the Euro-Mediterranean context. *Energy and Buildings, 223*, Article 110171. https://doi.org/10.1016/j.enbuild.2020.110171

Bassolino, E., D'Ambrosio, V., & Sgobbo, A. (2021). Data exchange processes for the definition of climate-proof design strategies for the adaptation to heatwaves in the urban open spaces of dense Italian cities. *Sustainability, 13*(10), 5694. https://doi.org/10.3390/su13105694

Bechtel, B., Alexander, P. J., Beck, C., Böhner, J., Brousse, O., Ching, J., Demuzere, M., Fonte, C., Gál, T., Hidalgo, J., Hoffmann, P., Middel, A., Mills, G., Ren, C., See, L., Sismanidis, P., Verdonck, M.-L., Xu, G., & Xu, Y. (2019). Generating WUDAPT level 0 data – Current status of production and evaluation. *Urban Climate, 27*, 24–45. https://doi.org/10.1016/j.uclim.2018.10.001

Bechtel, B., & Daneke, C. (2012). Classification of local climate zones based on multiple earth observation data. *IEEE Journal of Selected Topics in Applied Earth Observations and Remote Sensing, 5*(4), 1191–1202. https://doi.org/10.1109/JSTARS.2012.2189873

Pont, M. B., & Haupt, P. (2023). *Spacematrix: Space, Density and Urban Form-revised edition*. TU Delft OPEN Publishing. https://doi.org/10.59490/mg.38

Bishop, C. M., & Nasrabadi, N. M (2006). *Pattern recognition and machine learning*. Springer.

Boccalatte, A., Fossa, M., Thebault, M., Ramousse, J., & Ménézo, C. (2023). Mapping the urban heat Island at the territory scale: An unsupervised learning approach for urban

planning applied to the Canton of Geneva. *Sustainable Cities and Society, 96*, Article 104677. https://doi.org/10.1016/j.scs.2023.104677
Bontje, M. (2005). *The challenge of planned urbanisation: urbanisation and national urbanisation policy in the Netherlands in a Northwest-European perspective*. Rozenberg Publishers.
Chen, S., Wong, N. H., Ignatius, M., Zhang, W., He, Y., Yu, Z., & Hii, D. J. C. (2022). ATLAS: Software for analysing the relationship between urban microclimate and urban morphology in a tropical city. *Building and Environment, 208*, Article 108591. https://doi.org/10.1016/j.buildenv.2021.108591
Ching, J., Mills, G., Bechtel, B., See, L., Feddema, J., Wang, X., Ren, C., Brousse, O., Martilli, A., Neophytou, M., Mouzourides, P., Stewart, I., Hanna, A., Ng, E., Foley, M., Alexander, P., Aliaga, D., Niyogi, D., Shreevastava, A., Bhalachandran, P., Masson, V., Hidalgo, J., Fung, J., Andrade, M., Baklanov, A., Dai, W., Milcinski, G., Demuzere, M., Brunsell, N., Pesaresi, M., Miao, S., Mu, Q., Chen, F., & Theeuwes, N. (2018). WUDAPT: An urban weather, climate, and environmental modeling infrastructure for the anthropocene. *Bulletin of the American Meteorological Society, 99*(9), 1907–1924. https://doi.org/10.1175/BAMS-D-16-0236.1
Dab'at, A. A., & Alqadi, S. (2024). The impact of urban morphology on energy demand of a residential building in a Mediterranean climate. *Energy and Buildings, 325*, Article 114989. https://doi.org/10.1016/j.enbuild.2024.114989
Dekker, G., De Klerk, L., Witsen, P. P., & van der Cammen, H. (2012). *The selfmade land: Culture and evolution of urban and regional planning in the Netherlands*. Spectrum.
Demuzere, M., Bechtel, B., Middel, A., & Mills, G. (2019). Mapping Europe into local climate zones. *Plos One, 14*(4), 1–27. https://doi.org/10.1371/journal.pone.0214474
Ding, C., & He, X. (2004). K-means clustering via principal component analysis. In *Proceedings of the Twenty-First International Conference on Machine Learning* (p. 29). https://doi.org/10.1145/1015330.1015408
Dirksen, M., Ronda, R. J., Theeuwes, N. E., & Pagani, G. A. (2019). Sky view factor calculations and its application in urban heat island studies. *Urban Climate, 30*, Article 100498. https://doi.org/10.1016/j.uclim.2019.100498
Elbondira, T. A., Tokimatsu, K., Asawa, T., & Ibrahim, M. G. (2021). Impact of neighborhood spatial characteristics on the microclimate in a hot arid climate – A field based study. *Sustainable Cities and Society, 75*, Article 103273. https://doi.org/10.1016/j.scs.2021.103273
Eldesoky, A. H., Gil, J., & Pont, M. B. (2022). Combining environmental and social dimensions in the typomorphological study of urban resilience to heat stress. *Sustainable Cities and Society, 83*, Article 103971. https://doi.org/10.1016/j.scs.2022.103971
Eldesoky, A. H. M., Colaninno, N., & Morello, E. (2019). Improving local climate zones automatic classification based on physic-morphological urban features. In *XIII CTV 2019 Proceedings: XIII International Conference on Virtual Cityand Territory: "Challenges and Paradigms of the Contemporary City": UPC, Barcelona, October 2-4, 2019. Centre de Politica de Sol i Valoracions*. UPC: CPSV/Universitat Politècnica de Catalunya.
García-León, D., Masselot, P., Mistry, M. N., Gasparrini, A., Motta, C., Feyen, L., & Ciscar, J. C. (2024). Temperature-related mortality burden and projected change in 1368 European regions: A modelling study. *The Lancet Public Health, 9*(9), E644–E653. https://doi.org/10.1016/S2468-2667(24)00179-8
Geiß, C., Leichtle, T., Wurm, M., Pelizari, P. A., Standfuß, I., Zhu, X. X., So, E., Siedentop, S., Esch, T., & Taubenböck, H. (2019). Large-area characterization of urban morphology—Mapping of built-up height and density using TanDEM-X and Sentinel-2 data. *IEEE Journal of Selected Topics in Applied Earth Observations and Remote Sensing, 12*(8), 2912–2927. https://doi.org/10.1109/JSTARS.2019.2917755
Geletič, J., & Lehnert, M. (2016). GIS-based delineation of local climate zones: The case of medium-sized Central European cities. *Moravian Geographical Reports, 24*(3), 2–12. https://doi.org/10.1515/mgr-2016-0012
Gewers, F. L., Ferreira, G. R., Arruda, H. F. D., Silva, F. N., Comin, C. H., Amancio, D. R., Costa, L., & da, F. (2021). Principal component analysis: A natural approach to data exploration. *ACM Computing Surveys (CSUR), 54*(4), 1–34. https://doi.org/10.1109/JSTARS.2019.2917755
Grimmond, C. S. B., & Oke, T. R. (1999). Aerodynamic properties of urban areas derived from analysis of surface form. *Journal of Applied Meteorology, 38*(9), 1262–1292. https://doi.org/10.1175/1520-0450(1999)038<1262:APOUAD>2.0.CO;2
Guo, N., Liang, X., & Meng, L. (2024). Evaluation of thermal effects on urban road spatial structure: A case study of Xuzhou, China. *Heliyon, 10*(17), Article e37244. https://doi.org/10.1016/j.heliyon.2024.e37244
Habib, M. M., Esch, M.van, Ham, M.van, & Timmermans, W. J (2025). High-Resolution Datasets for Urban Heat Vulnerability Assessment in Urbanized Areas of the Netherlands. *Data in Brief, 60*, Article 111525. https://doi.org/10.1016/j.dib.2025.111525
Hamdy, M., Carlucci, S., Hoes, P. J., & Hensen, J. L (2017). The impact of climate change on the overheating risk in dwellings—A Dutch case study. *Building and Environment, 122*, 307–323. https://doi.org/10.1016/j.buildenv.2017.06.031
Hidalgo, J., Dumas, G., Masson, V., Petit, G., Bechtel, B., Bocher, E., Foley, M., Schoetter, R., & Mills, G. (2019). Comparison between local climate zones maps derived from administrative datasets and satellite observations. *Urban Climate, 27*, 64–89. https://doi.org/10.1016/j.uclim.2018.10.004
Intergovernmental Panel on Climate Change (IPCC). (2023). Weather and Climate Extreme Events in a Changing Climate. *Climate Change 2020 – The Physical Science Basis: Working Group I Contribution to the Sixth Assessment Report of the Intergovernmental Panel on Climate Change* (pp. 1513–1766). Cambridge University Press. https://doi.org/10.1017/9781009157896.013
Iqbal, N., Ravan, M., Mitraka, Z., Birkmann, J., Grimmond, S., Hertwig, D., Chrysoulakis, N., Somarakis, G., & Wendnagel-Beck, A. (2024). How does perceived heat stress differ between urban forms and human vulnerability profiles?–case study Berlin. *EGUsphere, 2024*, 1–27. https://doi.org/10.5194/egusphere-2024-1907
Javadpoor, M., Sharifi, A., & Gurney, K. R. (2024). Mapping the relationship between urban form and CO2 emissions in three US cities using the Local Climate Zones (LCZ) framework. *Journal of Environmental Management, 370*, Article 122723. https://doi.org/10.1016/j.jenvman.2024.122723
Jolliffe, I. T., & Cadima, J. (2016). Principal component analysis: A review and recent developments. *Philosophical transactions of the royal society A: Mathematical, Physical and Engineering Sciences, 374*(2065), Article 20150202. https://doi.org/10.1098/rsta.2015.0202
Joshi, M. Y., Rodler, A., Musy, M., Guernouti, S., Cools, M., & Teller, J. (2022). Identifying urban morphological archetypes for microclimate studies using a clustering approach. *Building and Environment, 224*, Article 109574. https://doi.org/10.1016/j.buildenv.2022.109574
Kennedy, J., Trewin, B., Betts, R., Thorne, P., Foster, P., Siegmund, P., … Alvar-Beltran, J. (2024). *State of the climate 2024: Update for COP29*. World Meteorological Organization.
Kenny, G. P., Tetzlaff, E. J., Journeay, W. S., Henderson, S. B., & O'Connor, F. K. (2024). Indoor overheating: A review of vulnerabilities, causes, and strategies to prevent adverse human health outcomes during extreme heat events. *Temperature, 11*(3), 203–246. https://doi.org/10.1080/23328940.2024.2361223
Kleerekoper, L., Kluck, J., & van den Dobbelsteen, A. (2017). Selection support framework fostering resilience based on neighbourhood typologies. *Climate Change Adaptation in North America: Fostering Resilience and the Regional Capacity to Adapt*, 321–335.
Klopfer, F. (2023). The thermal performance of urban form – An analysis on urban structure types in Berlin. *Applied Geography, 152*, Article 102890. https://doi.org/10.1016/j.apgeog.2023.102890
Kluck, J., Kleerekoper, L., aura, Erwin, S., Corpel, L., Bons, P., Arif, Z., Geisler, L., Veenbos, K., & Koekoek, A. (2023). *Computer leert wijktypen bepalen voor heel Nederland: Een studie naar het inzetten van kunstmatige intelligentie voor het bepalen van wijktypen*. Climate Adaptation Services.
Kolokotsa, D., Lilli, K., Gobakis, K., Mavrigiannaki, A., Haddad, S., Garshasbi, S., Mohajer, H. R. H., Paolini, R., Vasilakopoulou, K., Bartesaghi, C., Prasad, D., & Santamouris, M. (2022). Analyzing the Impact of urban planning and building typologies in urban heat Island mitigation. *Buildings, 12*(5), 537. https://doi.org/10.3390/buildings12050537
Koopmans, S., Heusinkveld, B. G., & Steeneveld, G. J. (2020). A standardized physical equivalent temperature urban heat map at 1-m spatial resolution to facilitate climate stress tests in the Netherlands. *Building and Environment, 181*, Article 106984. https://doi.org/10.1016/j.buildenv.2020.106984
Li, Y., Schubert, S., Kropp, J. P., & Rybski, D. (2020). On the influence of density and morphology on the Urban Heat Island intensity. *Nature Communications, 11*(1), 2647. https://doi.org/10.1038/s41467-020-16461-9
Lin, L., Deng, Y., Peng, M., Zhen, L., & Qin, S. (2023). Multi-Scale influence analysis of urban shadow and spatial form features on urban thermal environment. *Remote Sensing, 15*(20), 4902. https://doi.org/10.3390/rs15204902
Lindberg, F., Grimmond, C. S. B., & Martilli, A. (2015). Sunlit fractions on urban facets – Impact of spatial resolution and approach. *Urban Climate, 12*, 65–84. https://doi.org/10.1016/j.uclim.2014.11.006
Liu, G., Zheng, Y., Wu, X., Che, Y., Zhang, H., Gao, J., & Liu, X. (2025). Assessing urban morphology effects on residential building electricity consumption via explainable machine learning: Evidence from China's hot summer and warm winter zone. *Energy and Buildings, 345*, Article 116063. https://doi.org/10.1016/j.enbuild.2025.116063
López-Guerrero, R. E., Verichev, K., Cardenas-Ramirez, J. P., & Carpio, M. (2024). Urban heat islands' effects on the thermo-energy performance of buildings according to their socio-economic factors. *Developments in the Built Environment, 20*, 100566. https://doi.org/10.1016/j.dibe.2024.100566
Ma, R., Li, X., & Chen, J. (2021). An elastic urban morpho-blocks (EUM) modeling method for urban building morphological analysis and feature clustering. *Building and Environment, 192*, Article 107646. https://doi.org/10.1016/j.buildenv.2021.107646
Maiullari, D., Esch, M. P., & Timmeren, A. (2021). A quantitative morphological method for mapping local climate types. *Urban Planning, 6*(3), 240–257. https://doi.org/10.17645/up.v6i3.4223
Martilli, A., Krayenhoff, E. S., & Nazarian, N. (2020). Is the urban heat island intensity relevant for heat mitigation studies? *Urban Climate, 31*, Article 100541. https://doi.org/10.1016/j.uclim.2019.100541
Masson, V., Heldens, W., Bocher, E., Bonhomme, M., Bucher, B., Burmeister, C., Munck, C.de, Esch, T., Hidalgo, J., Kanani-Sühring, F., Kwok, Y.-T., Lemonsu, A., Lévy, J.-P., Maronga, B., Pavlik, D., Petit, G., See, L., Schoetter, R., Tornay, N., Votsis, A., & Zeidler, J. (2020). City-descriptive input data for urban climate models: Model requirements, data sources and challenges. *Urban Climate, 31*, Article 100536. https://doi.org/10.1016/j.uclim.2019.100536
Meiyan Zhao, Z. Q., Hongyan, Cai, & Xu, X. (2016). Influence of urban expansion on the urban heat island effect in Shanghai. *International Journal of Geographical Information Science, 30*(12), 2421–2441. https://doi.org/10.1080/13658816.2016.1178389
Middel, A., Lukasczyk, J., Maciejewski, R., Demuzere, M., & Roth, M. (2018). Sky view factor footprints for urban climate modeling. *Urban Climate, 25*, 120–134. https://doi.org/10.1016/j.uclim.2018.05.004
Murphy, K. P. (2022). *Probabilistic machine learning: an introduction*. MIT press.
Nabielek, K. (2012). The compact city: Planning strategies, recent developments and future prospects in the Netherlands. *Paper presented at the 26th Annual Congress of the Association of European Schools of Planning*. Ankara, Turkey: (AESOP).
Oke, T. R., Mills, G., Christen, A., & Voogt, J. A. (2017). *Urban climates*. Cambridge university press.
Oke, T. R. (1978). *Boundary layer climates*. Routledge.

Openshaw, S. (1984). The modifiable areal unit problem. *Concepts and techniques in modern geography*.
Palme, M., & Salvati, A. (2021). *Urban microclimate modelling for comfort and energy studies*. Springer.
Peeters, A., & Etzion, Y. (2012). Automated recognition of urban objects for morphological urban analysis. *Computers, Environment and Urban Systems, 36*(6), 573–582. https://doi.org/10.1016/j.compenvurbsys.2012.05.002
Priemus, H. (2018). How housing, infrastructure and water determined the spatial structure of the Randstad. *European Planning Studies, 26*, 546–570. https://doi.org/10.1080/09654313.2017.1402867
Rahmani, N., & Sharifi, A. (2025). Urban heat dynamics in local climate zones (LCZs): A systematic review. *Building and Environment, 267*, Article 112225. https://doi.org/10.1016/j.buildenv.2024.112225
Rodler, A., & Leduc, T. (2019). Local climate zone approach on local and micro scales: Dividing the urban open space. *Urban Climate, 28*, Article 100457. https://doi.org/10.1016/j.uclim.2019.100457
Schirmer, P. M., & Axhausen, K. W. (2019). A multiscale clustering of the urban morphology for use in quantitative models. In L. D'Acci (Ed.), *The mathematics of urban morphology* (pp. 355–382). Springer International Publishing. https://doi.org/10.1007/978-3-030-12381-9_16.
Souch, C., & Grimmond, S. (2006). Applied climatology: urban climate. *Progress in physical geography, 30*(2), 270–279.
Steeneveld, G.-J., Klompmaker, J. O., Groen, R. J. A., & Holtslag, A. A. M. (2018). An urban climate assessment and management tool for combined heat and air quality judgements at neighbourhood scales. *Resources, Conservation and Recycling, 132*, 204–217. https://doi.org/10.1016/j.resconrec.2016.12.002
Stewart, I. D., & Oke, T. R. (2012). Local climate zones for urban temperature studies. *Bulletin of the American Meteorological Society, 93*(12), 1879–1900. https://doi.org/10.1175/BAMS-D-11-00019.1
Sützl, B. S., Strebel, D. A., Rubin, A., Wen, J., & Carmeliet, J. (2024). Urban morphology clustering analysis to identify heat-prone neighbourhoods in cities. *Sustainable Cities and Society, 107*, Article 105360. https://doi.org/10.1016/j.scs.2024.105360
Tardioli, G., Kerrigan, R., Oates, M., O'Donnell, J., & Finn, D. P. (2018). Identification of representative buildings and building groups in urban datasets using a novel pre-processing, classification, clustering and predictive modelling approach. *Building and Environment, 140*, 90–106. https://doi.org/10.1016/j.buildenv.2018.05.035
Taubenböck, H., Kraff, N. J., & Wurm, M. (2018). The morphology of the arrival city - A global categorization based on literature surveys and remotely sensed data. *Applied Geography, 92*, 150–167. https://doi.org/10.1016/j.apgeog.2018.02.002
Theeuwes, N. E., Steeneveld, G.-J., Ronda, R. J., & Holtslag, A. A. (2017). A diagnostic equation for the daily maximum urban heat island effect for cities in northwestern Europe. *International Journal of Climatology, 37*, 443–454. https://doi.org/10.1002/joc.4717
Thravalou, S., Mouzourides, P., Michael, A., Philokyprou, M., & Neophytou, M. (2021). A Field study on the environmental conditions of street canyons in dense, historic, and urban centres in the mediterranean. The Case of Nicosia, Cyprus. In *Euro-Mediterranean Conference for Environmental Integration* (pp. 637–640). Cham: Springer Nature Switzerland. https://doi.org/10.1007/978-3-031-43922-3_143.
Ullmann, T., Hennig, C., & Boulesteix, A. L. (2022). Validation of cluster analysis results on validation data: A systematic framework. *Wiley Interdisciplinary Reviews: Data Mining and Knowledge Discovery, 12*(3), e1444.
Verdonck, M. L., Okujeni, A., S.van der, Linden, Demuzere, M., Wulf, R. D., & Coillie, F. V (2017). Influence of neighbourhood information on 'Local Climate Zone' mapping in heterogeneous cities. *International Journal of Applied Earth Observation and Geoinformation, 62*, 102–113. https://doi.org/10.1016/j.jag.2017.05.017
Villaverde, A., Álvarez, I., Rojí, E., & Garmendia, L. (2024). Categorisation of urban open spaces for heat adaptation: A cluster based approach. *Building and Environment, 263*, Article 111861. https://doi.org/10.1016/j.buildenv.2024.111861
Wang, J., & Biljecki, F. (2022). Unsupervised machine learning in urban studies: A systematic review of applications. *Cities, 129*, Article 103925. https://doi.org/10.1016/j.cities.2022.103925
Wu, H., Ming, Y., & Liu, Y. (2024). Investigating the influence of morphologic and functional polycentric structures on urban heat island: A case of Chongqing, China. *Sustainable Cities and Society, 114*, Article 105790. https://doi.org/10.1016/j.scs.2024.105790
Wu, Y., Mashhoodi, B., Patuano, A., Lenzholzer, S., Zertuche, L. N., & Acred, A. (2022). Heat-prone neighbourhood typologies of European cities with temperate climate. *Sustainable Cities and Society, 87*, Article 104174. https://doi.org/10.1016/j.scs.2022.104174
Xiao, J., Lu, J., & Li, X. (2017). Davies bouldin index based hierarchical initialization k-means. *Intelligent Data Analysis, 21*(6), 1327–1338. https://doi.org/10.3233/IDA-163129
Yang, X., Zhao, L., Bruse, M., & Meng, Q. (2013). Evaluation of a microclimate model for predicting the thermal behavior of different ground surfaces. *Building and Environment, 60*, 93–104. https://doi.org/10.1016/j.buildenv.2012.11.008
Yin, S., Lang, W., & Xiao, Y. (2019). The synergistic effect of street canyons and neighbourhood layout design on pedestrian-level thermal comfort in hot-humid area of China. *Sustainable Cities and Society, 49*, Article 101571. https://doi.org/10.1016/j.scs.2019.101571
Yu, T., Sützl, B. S., & van Reeuwijk, M. (2023). Urban neighbourhood classification and multi-scale heterogeneity analysis of Greater London. *Environment and Planning B: Urban Analytics and City Science, 50*(6), 1534–1558. https://doi.org/10.1177/23998083221140890
Zendeli, D., Colaninno, N., Maiullari, D., Esch, M.van, Timmeren, A.van, Marconi, G., Bonora, R., & Morello, E. (2025). From heatwaves to 'healthwaves': A spatial study on the impact of urban heat on cardiovascular and respiratory emergency calls in the city of Milan. *Sustainable Cities and Society, 124*, Article 106181. https://doi.org/10.1016/j.scs.2025.106181
Zhang, M., You, W., Qin, Q., Peng, D., Hu, Y., Gao, Z., & Buccolieri, R. (2022). Investigation of typical residential block typologies and their impact on pedestrian-level microclimate in summers in Nanjing, China. *Frontiers of Architectural Research, 11*(2), 278–296. https://doi.org/10.1016/j.foar.2021.10.008
Zhang, X., Steeneveld, G. J., Zhou, D., Duan, C., & Holtslag, A. A. M. (2019). A diagnostic equation for the maximum urban heat island effect of a typical Chinese city: A case study for Xi'an. *Building and Environment, 158*, 39–50. https://doi.org/10.1016/j.buildenv.2019.05.004
Zhang, Y., Balzter, H., & Li, Y. (2021). Influence of Impervious Surface Area and Fractional Vegetation Cover on Seasonal Urban Surface Heating/Cooling Rates. *Remote Sensing, 13*(7), 1263. https://doi.org/10.3390/rs13071263